MnO_2/Co_3O_4 COMPOSITE ELECTRODES FOR POTENTIAL SUPERCAPACITOR APPLICATIONS

A. Benashvili*, N. Nioradze, D. Tediashvili, L. Rokva

Rafael Agladze Institute of Inorganic Chemistry and Electrochemistry, Ivane Javakhishvili Tbilisi StateUniversity, 11 Mindeli Str., 0186 Tbilisi, Georgia

e-mail: Archilbenashvili69@gmail.com

Abstract: *As the global energy landscape shifts toward more sustainable and high-performance storage solutions, the development of next-generation supercapacitor electrodes has become increasingly critical. Addressing this demand, we developed a straightforward chemical co-precipitation method to synthesize manganese dioxide (MnO_2) and cobalt oxide (Co_3O_4), incorporating a conductive carbon framework as a potential electrode material for supercapacitors. The resulting mixture was further combined with poly(3,4-ethylenedioxythiophene) (PEDOT) and deposited onto a nickel foam/graphene monolayer substrate to fabricate test electrodes. This method bypasses the complexity of multi-step fabrication and post-processing, offering a streamlined, scalable approach to building multifunctional hybrid electrodes. The resulting composite exhibits rapid ion transport and enhanced charge storage, while Energy-Dispersive X-ray spectroscopy (EDS) confirmed the successful incorporation of Mn and Co elements. Furthermore, X-ray diffraction (XRD) patterns indicated that the composite possesses an amorphous structure. Cyclic Voltammetry (CV) and Galvanic Charge/Discharge (GCD) measurements revealed excellent long-term cycling stability, indicating the viability of the fabricated composite for potential supercapacitor applications. Electrochemical Impedance Spectroscopy (EIS) was also performed to evaluate the internal resistance and charge-transfer properties, providing complementary insight into the electrode's electrochemical behavior.*
Keywords: *Electrochemical characterization, excellent stability, Cyclic Voltammetry, Specific capacitance, Thermal behavior.*

Introduction

Supercapacitors, also known as electrochemical capacitors or ultracapacitors, represent a promising class of energy storage devices characterized by high power density, fast charge/discharge rates, and long cycling life. These characteristics make them particularly attractive for use in fields such as portable electronics, electric vehicles, aerospace systems, and technologies for the integration and management of renewable energy sources [1, 2]. Despite their advantages, supercapacitors typically suffer from lower energy density compared to conventional batteries. This limitation is largely attributed to the nature of their energy storage mechanism - either through electrostatic charge accumulation in electric double-layer capacitors (EDLCs) or fast faradaic reactions in pseudocapacitors [3]. One of the primary challenges in supercapacitor research is the development of advanced electrode materials that can enhance both - energy and power density without compromising stability.

Transition metal oxides (TMOs) have received significant attention as pseudocapacitive materials due to their high theoretical capacitance and ability to undergo fast reversible redox reactions. Among TMOs, manganese dioxide (MnO_2) and cobalt oxide (Co_3O_4) are widely studied. MnO_2 is particularly attractive due to theoretical capacitance values up to ~1370 F/g, but its poor electrical conductivity and limited cycle life limit its practical applications [4]. Co-based oxides, by contrast, exhibit superior electrical conductivity and structural robustness. Among them, Co_3O_4 possesses a high practical specific capacitance (~600 F/g), low cost, environmental friendliness, and good chemical stability, making it a promising active material for supercapacitor applications [5]. However, its capacitance in practical applications is considerably lower than the theoretical value (~3560 F/g) [1]. This discrepancy arises mainly from hindered electron transfer due to low intrinsic conductivity, sluggish ion diffusion kinetics, significant volume expansion/contraction during cycling, and severe particle aggregation. Consequently, both the capacitance and cycling stability of Co_3O_4 electrodes remain limited [6, 7].

Researchers have developed composite materials that combine TMOs with conductive carbonaceous materials such as graphene, carbon nanotubes (CNTs), or activated carbon. These carbon frameworks further enhance the electronic conductivity and provide mechanical reinforcement to the metal oxides. Additionally, the incorporation of conductive polymers such as polyaniline (PANI), polypyrrole (PPy), or poly(3,4-ethylenedioxythiophene) (PEDOT) improves electrochemical performance by contributing additional pseudocapacitance and structural flexibility [8]. Numerous studies have demonstrated the superior performance of hybrid electrodes based on MnO_2/graphene, Co_3O_4/CNT, or MnO_2/PANI composites. These systems show improvements in specific capacitance, rate capability, and cycling stability [9] [10]. However, some of these approaches involve complicated synthesis methods or poor long-term performance, which limit their industrial applications [11].

Exploration of hybrid systems involving manganese and cobalt oxides has opened new pathways for developing next-generation electrode materials with enhanced electrochemical characteristics. For instance, innovative hybrid MnO_2/Co_3O_4 core–shell nanowire arrays were developed for electrochemical capacitors, achieving a specific capacitance of 480 F/g and excellent cycling stability, with only a 2.7% loss after 5000 cycles [12]. Polyaniline–manganese dioxide (PANI–MnO_2) composites with varying compositions were prepared via in situ chemical oxidative polymerization of aniline in an acidic aqueous medium, where MnO_2 was formed through the reaction of $MnSO_4$ with $KMnO_4$. The resulting specific capacitance ranged from 99 to 242 F/g at a current density of 0.10 A/g over a potential window of 0.0–0.8 V [13]. Nanostructured Co-doped Mn_3O_4 spinel (Co, Mn_3O_4) was synthesized via co-precipitation under O_3 oxidizing conditions, followed by post-heat treatment. A maximum specific capacitance of 2701 F/g was obtained at 5 A/g within 0.01–0.55 V vs. Hg/HgO in 6 M KOH. Even at a high current density of 30 A/g, the capacitance remained 1537.2 F/g (56.9%), indicating excellent rate capability. After 500 cycles at 20 A/g, the specific capacitance was retained at 1324 F/g (76.4%) [14]. MnO_2/GO, NiO/GO, and MnO_2/NiO/GO electrodes were hydrothermally fabricated, incorporating graphene oxide (GO) to reduce electrical resistance. The synergistic effect of the components with GO enhanced electrode performance, durability, and mechanical strength. Specific capacitances measured by GCD were 773, 487, and 1141 F/g for MnO_2/GO, NiO/GO, and MnO_2/NiO/GO, respectively [15]. MnO_2 and Co_3O_4 were uniformly wrapped around superaligned electrospun carbon nanofibers (SA-ECNFs), creating a porous morphology that improved energy storage through both pseudocapacitance and electrochemical double-layer capacitance. The resulting MnO_2/Co_3O_4/SA-ECNFs electrode exhibited a specific capacitance of 728 F/g in 6 M KOH (CV) compared to 622 F/g for MnO_2/SA-ECNFs at 5 mV/s. GCD measurements revealed an energy density of 64.5 Wh/kg, a power density of 1276 W/kg, and 71.8% capacity retention over 11000 cycles [16].

While the literature often reports exceptionally high specific capacitance values, some studies have observed relatively modest electrochemical performance. Nevertheless, such findings should not be overlooked, as they frequently emphasize other beneficial characteristics of the materials, including structural stability, cost-effectiveness, ease of synthesis, or practical applicability under real-world conditions. In one such study, MnO_2/C composites delivered a maximum specific capacitance of 922.67 mF/g, along with a power density of 90.15 W/kg and an energy density of 0.063 Wh/kg [17]. Although these values are lower than those achieved by record-breaking capacitances of other MnO_2-based systems, the study highlights the practical viability of the material, suggesting that performance metrics should be evaluated in conjunction with broader considerations relevant to device integration and scalability.

In our work, we developed novel composite electrodes by combining manganese oxide (MnO_2) and cobalt oxide (Co_3O_4), further integrating the mixture with the conductive polymer PEDOT and applying it onto a nickel foam/graphene monolayer substrate. To probe their influence on electrochemical and thermal behavior, we incorporated carbon nanotubes (CNT) in one case and CNT together with graphene oxide (GO) in another. Our electrochemical characterization revealed that the composite containing both CNT and GO exhibited better performance than other samples in terms of specific capacitance, energy density, and power density. Compared with the methods described here,

the principal advantage of our method is its simplicity and scalability. The synthesis route enables the preparation of high-performance electrodes without complex multi-step procedures or harsh experimental conditions. Our approach ensures excellent cycling stability, cost-effectiveness, and environmental compatibility.

Experimental Part

Materials. Reagents, including Nickel Foam/Graphene Monolayer (purity ≥99.9%, thickness ~1.6 mm, porosity ~95%, pore size ~450 μm), manganese sulfate monohydrate ($MnSO_4 \cdot H_2O$ purity: ≥99%), cobalt sulfate heptahydrate ($CoSO_4 \cdot 7H_2O$ purity: ≥99%), sodium sulfate (Na_2SO_4 purity: ≥99%), poly(3,4-ethylenedioxythiophene) (PEDOT 3.0-4.0% in H_2O, high-conductivity grade) were purchased from Sigma-Aldrich and used without further purification. Carbon nanotubes (CNT) and nanographene oxide (GO diameter: 90 nm-200 nm, thickness: about 1 nm, single-layer ratio: >99% purity: >99%) were obtained from Graphene Supermarket, also without further purification. Deionized water (resistivity ≥18.2 MΩ·cm) was used throughout all experiments.

Synthesis of MnO_2/Co_3O_4 powders. MnO_2/Co_3O_4 powders were synthesized via a simple co-precipitation method followed by calcination. This type of synthesis process, involving an $MnSO_4 \bullet H_2O/CoSO_4 \bullet 7H_2O$ mixture and NaOH, NH_4OH, or Na_2CO_3 as a precipitating agent, is well known in the literature for preparing mixed metal oxide composites used in energy storage, catalysis, and electrochemical applications [18][19]. In our experiment, aqueous solutions of $MnSO_4 \bullet H_2O$ (0.1 M) and $CoSO_4 \bullet 7H_2O$ (0.1 M) were prepared, and NaOH solution was subsequently added dropwise under continuous stirring until the pH reached 10–11, resulting in the formation of a mixed $Mn(OH)_2/Co(OH)_2$ precipitate at room temperature. The obtained precipitate was dried at 80–100°C and then calcined in an oven at 700°C for 2 h [20]. During the calcination process, Mn and Co hydroxides were oxidized to MnO_2 and Co_3O_4, respectively, yielding the final MnO_2/Co_3O_4 powder.

Fabrication of electrodes. Before electrode fabrication, the synthesized MnO_2/Co_3O_4 powder was rinsed with deionized water and dried naturally at room temperature. The resulting material was then mixed with PEDOT solution and deposited onto nickel foam/graphene monolayer using the spin-coating technique (1500 rpm for 30 s), followed by ambient drying. Three working electrode configurations were prepared. In the first configuration, the synthesized MnO_2/Co_3O_4 powder was blended with PEDOT and directly coated onto nickel foam with a graphene monolayer. In the second step, the mixture of MnO_2/Co_3O_4 (70 wt%) and commercial CNT (30 wt%) was blended with PEDOT before coating. Finally, the third powder configuration consisted of MnO_2/Co_3O_4 (70 wt%), commercial CNT (20 wt%), and commercial GO (10 wt%) mixed with PEDOT before deposition. In all cases, the geometric electrode area was fixed at 5×5 mm, with an active material loading of approximately 3 mg.

Electrochemical measurements. All electrochemical measurements were performed in a three-electrode cell configuration using a CHI660C electrochemical workstation (CH Instruments, USA). The working electrodes, prepared as described in section (2.3), were based on nickel foam coated with a graphene monolayer and loaded with one of the three active material composites. A platinum wire was used as the counter electrode, while an Ag/AgCl/3M KCl served as a reference electrode. Naturally aerated aqueous 0.5 M Na_2SO_4 was used as an electrolyte.

Structural and elemental characterization. A Zeiss Sigma 300 Field Emission Scanning Electron Microscope (FESEM) equipped with a Bruker Energy Dispersive Spectrometer (EDS) was used to analyze the morphology and composition of the synthesized materials, and an accelerating voltage of 15 kV was used to capture the images.

XRD was performed with Cu Kα radiation (λ=0.15406 nm) at 30 kV and 8 mA with a graphite monochromator (d=3.358 Å). The scans were conducted at a rate of 4° per minute in continuous mode.

Thermal Analysis. Thermal stability was assessed using thermal gravimetric analysis (TGA) with an STA 2500 Regulus system from room temperature to 1000°C at a heating rate of 10°C/min under air atmosphere.

Results and Discussion

The structure of the composite suggests a potentially porous morphology. Such architecture is generally advantageous for electrode materials in supercapacitors, as it can facilitate ion diffusion, increase the electrochemically active surface area for reactions, and enhance electrolyte accessibility, thereby improving overall charge storage performance [21].

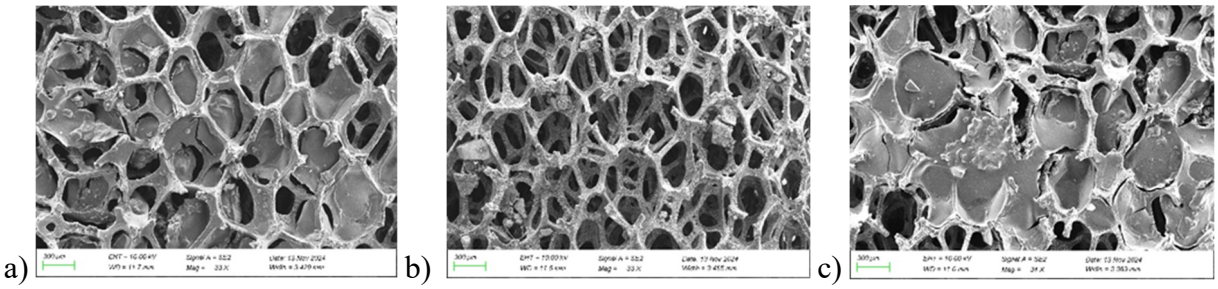

Fig. 1. SEM images of electrode materials: a) MnO_2/Co_3O_4; b) MnO_2/Co_3O_4/CNT; c) MnO_2/Co_3O_4/CNT/GO.

XRD analysis of the powder indicates that the sample is predominantly amorphous. The X-ray fluorescence (XRF) spectrum of the MnO_2/Co_3O_4 composite confirms the presence of manganese and cobalt as the major elements, with MnKα appearing as the dominant peak, followed by characteristic CoKα and MnKβ signals, supporting the successful incorporation of both metal oxides into the sample.

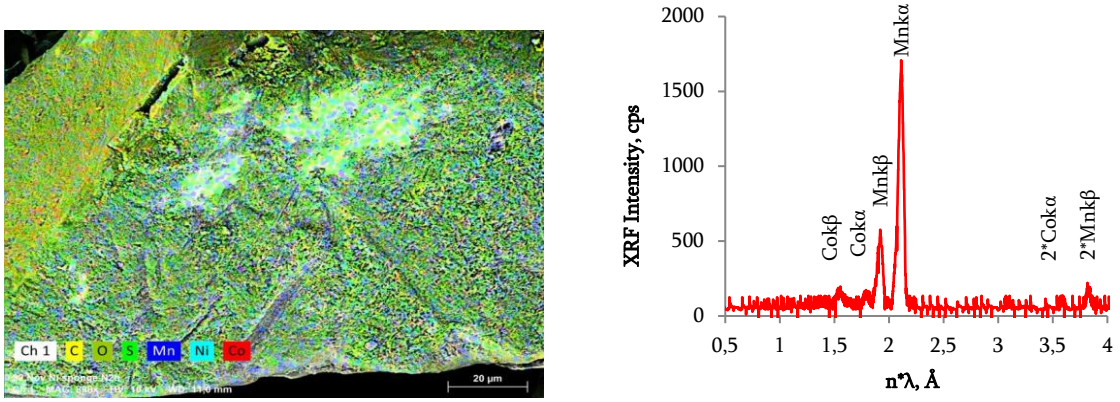

Fig. 2. a) EDS elemental mapping analysis of the electrode material and b) XRF curve of an electrode material.

The thermogravimetric behavior of the MnO_2/Co_3O_4 composite has been extensively studied in different variations in studies [22] and [23]. In our experiments, the analysis revealed several-step weight-loss events, which were comparatively more evident in the MnO_2/Co_3O_4–carbon composites. The initial decrease below ~200 °C, observed in all samples, is attributed to the evaporation of adsorbed moisture and residual volatiles, as evidenced by Differential Thermal Analysis (DTA) peaks appearing in the ~100–200 °C range. For the pristine MnO_2/Co_3O_4 sample, the weight loss after this region up to ~780 °C can be attributed mainly to the gradual release of residual hydroxyl or oxygen-containing groups, as well as lattice oxygen from the mixed metal oxides [24]. Notably, this sample retained the highest residue (~86%), highlighting the predominance of thermally stable transition metal oxides.

CNT- and CNT/GO-modified composites demonstrated slightly lower final mass retention (~76 % and ~65 %, respectively), reflecting the contribution of carbonaceous components, which decompose progressively from ~300 °C until the end of the process, as evidenced by the thermogravimetric (TG) curves. Several DTA peaks observed in these samples correspond to the

combustion of carbon components and to phase transformations of the metal oxides within the carbon framework [25].

By comparison, no distinct DTA peaks were observed for the pristine MnO_2/Co_3O_4 sample above 200°C, indicating the absence of pronounced endothermic or exothermic processes. This behavior suggests that the pure oxide system exhibits a relatively stable thermal response without major phase transformations or decomposition events. Such stability is attributed to the strong metal/oxygen bonding within the MnO_2/Co_3O_4 lattice and the lack of additional carbonaceous or polymeric components that could induce thermal oxidation or reduction reactions, which typically generate noticeable DTA signals.

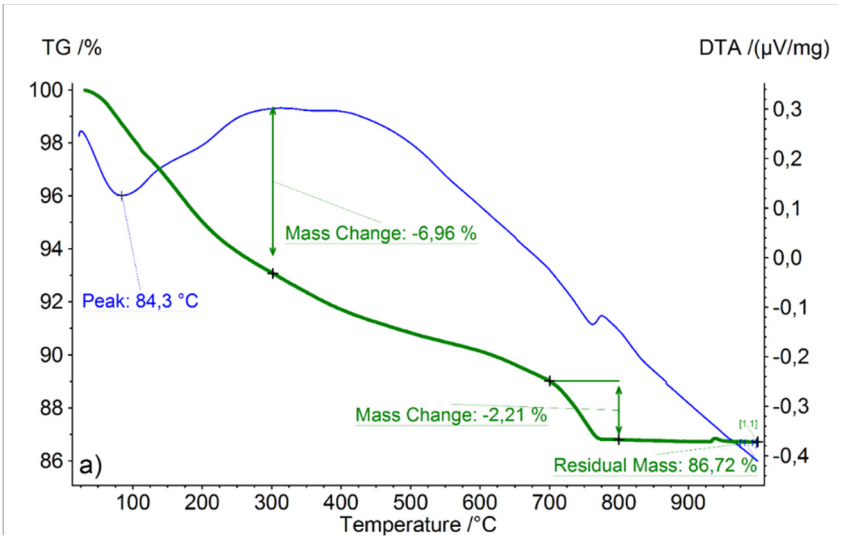

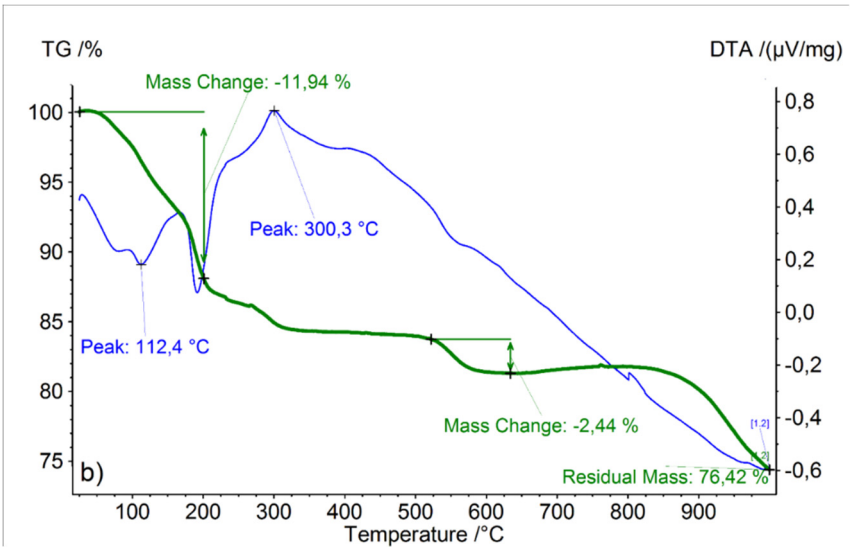

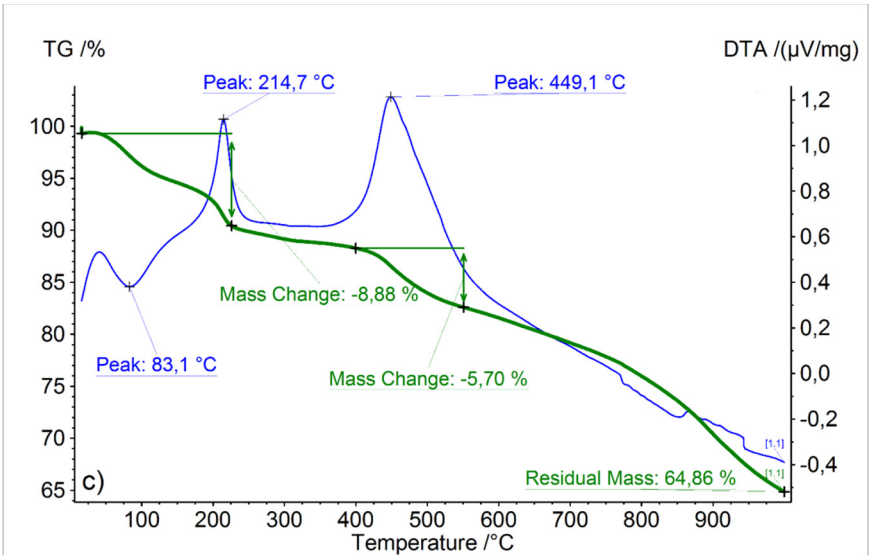

Fig. 3. The thermogravimetric curves of a) MnO_2/Co_3O_4 powder; b) MnO_2/Co_3O_4/CNT powder; c) MnO_2/Co_3O_4/CNT/GO powder.

Cyclic voltammetry (CV) measurements were conducted at scan rates of 0.1 V/s, 0.05 V/s, 0.01 V/s, 0.005 V/s, and 0.001 V/s. As shown in Fig. 4, the CV curves for the PEDOT + MnO_2/Co_3O_4/CNT/GO composite demonstrate a higher current response compared to the composites PEDOT+MnO_2/Co_3O_4 and PEDOT+MnO_2/Co_3O_4/CNT/ indicating enhanced capacitive behavior with GO. The shapes of the CV curves demonstrate pseudocapacitive behavior associated with the underlying redox processes. At higher scan rates in CV measurements, the capacitive current may be overestimated due to non-ideal capacitive behavior and additional faradaic contributions, leading to inflated capacitance values. Faster scans may also distort the current response and reduce the influence of diffusion limitations, resulting in an apparent increase in capacitance [26, 27]. Samples incorporating a carbon framework maintained excellent stability even after 5000 cycles, whereas the pristine MnO_2/Co_3O_4 material displayed a noticeable difference between the initial and final CV profiles, suggesting gradual structural degradation and loss of active sites during cycling.

Fig. 4. CV curves of composites: a) CV curves for all three composite electrodes at 0.05 V/s scan rate and b) CV curves of PEDOT + MnO_2/Co_3O_4/CNT/GO composite electrode at various scan rates.

Unlike CV, which involves sweeping the potential at variable scan rates, the GCD technique operates under a constant current, offering a more direct and practical assessment of the charge storage performance under real operating conditions [28, 29]. The GCD profiles obtained in this study

further confirm the superior electrochemical reversibility and Coulombic efficiency of the carbon-based electrodes. The CNT/GO-containing composite exhibited outstanding cyclic stability, retaining its initial performance even after 5000 continuous charge-discharge cycles, while maintaining a nearly ideal triangular curve shape. As presented in Fig.5b, the slight deviations from the perfect triangular shape observed in the other two samples indicate the presence of faradaic redox processes, which are typical characteristics of pseudocapacitive materials [30].

The specific capacitance derived from the GCD measurements was calculated using Eq. (1):

$$C_{sp} = \frac{I\Delta t}{m\Delta V} \ F/g \qquad (1)$$

Where C_{sp} denotes the specific capacitance (F/g), I is the discharge current (0.1 mA), Δt represents the discharge time (90 s for PEDOT + MnO_2/Co_3O_4/CNT/GO, 70 s for PEDOT + MnO_2/Co_3O_4/CNT and 35 s for PEDOT + MnO_2/Co_3O_4), m is the mass of the active material (~3.4 mg), and ΔV is the potential window (0.45 V in all cases). The specific capacitance was 5.88 F/g for the PEDOT + MnO_2/Co_3O_4/CNT/GO containing electrode, while values of 3.94 F/g and 2,11 F/g were obtained for the MnO_2/Co_3O_4/CNT and MnO_2/Co_3O_4-containing electrodes, respectively. The energy density was obtained from Eq. (2):

$$E = \frac{0.5C_{sp}(\Delta V)^2}{3.6} \ Wh/kg \qquad (2)$$

Where E - is energy density (Wh/kg).
The GCD curves also enabled the calculation of power density via Eq. (3):

$$P = \frac{Ex3600}{\Delta t} \ W/kg \qquad (3)$$

Where P is power density (W/kg), 3600 is the conversion factor for hours to seconds. The PEDOT + MnO_2/Co_3O_4/CNT/GO material demonstrated an energy density (E) of 0.17 Wh/kg and a power density (P) of 6.62 W/kg; the PEDOT + MnO_2/Co_3O_4/CNT material demonstrated an energy density (E) of 0.11 Wh/kg and a power density (P) of 5.62 W/kg; and the PEDOT + MnO_2/Co_3O_4 material demonstrated an energy density (E) of 0.05 Wh/kg and a power density (P) of 5.14 W/kg.

The equations presented here are fundamental for investigating the electrochemical characteristics of supercapacitors, and their application is widely found in the calculations reported in references [1, 2, 5, 9, 10, 14, 29]. However, all three equations are presented together specifically in reference [15].

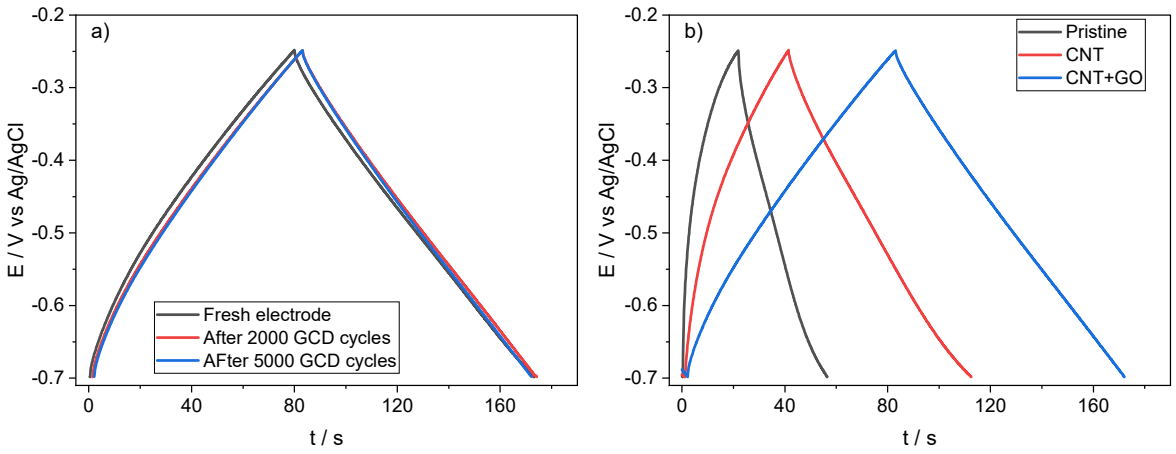

Fig. 5. GCD measurements of the electrodes. a) GCD curves of PEDOT + MnO_2/Co_3O_4/CNT/GO composite electrode and b) GCD curves of last cycle all three composite electrodes

To further characterize the electrode's capacitive properties, as well as study its degradation during different modes of cycling, the Electrochemical Impedance Spectroscopy (EIS) technique was employed. The measurements were carried out at open-circuit potential, with the 15 mV excitation amplitude. The materials used in this study are the same as those employed for CV and GCD measurements and are listed in section (2.4). One of the most important decisions to make is to correctly pick an equivalent circuit to fit, as it determines the values calculated. The appropriate circuits have been discussed in literature [31, 32]. Typically, in terms of mathematical fit, multi-element circuits are better (i.e., lowest error for calculated values); however, in that case, interpreting the data might become challenging. In our case, we were interested in potential degradation of the materials during prolonged cycling and build-up of decomposition products on the surface of the electrode. These processes affect the performance twofold: i) degradation of the material may lead to the reduction of the surface area, and ii) build-up of amorphous, electrochemically inactive materials further reduces Electrochemically Active surface area (ECSA). Fortunately, both of the processes can be captured by increased charge transfer resistance; therefore, a relatively simple circuit was selected in this work (Fig. 6).

This circuit has 2 elements, one to represent the electrochemically active material itself and the other to account for any impurities, which may be present in a sample as a synthesis by-product as well as accumulate due to the degradation. This second element will be denoted as R1 further and will be used as a metric to evaluate the extent of the degradation and by-product accumulation on the surface. Measurements for the single electrode were conducted twice: on a freshly prepared sample and after 5000 cycles in different modes (either CV or GCD). For clarity and brevity, here we only present the raw data for one electrode—PEDOT+MnO_2/Co_3O_4/CNT (3 GCD). This sample is particularly interesting as it seems to have retained almost all capacitive properties after over 5000 GCD cycles.

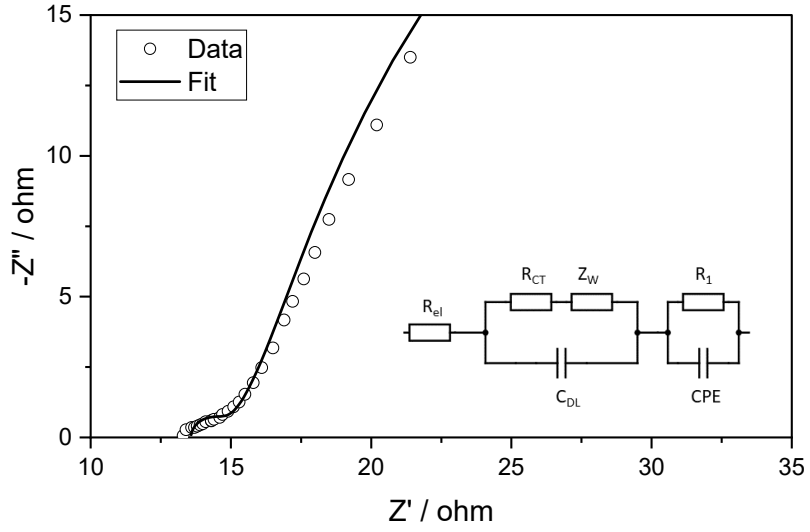

Fig. 6. EIS measurement for the electrode. The equivalent circuit is presented on a figure as an inset.

The EIS measurements, similar to CVs discussed previously, reveal a typical pattern for the double-layer/pseudocapacitive electrodes [33]. In the equivalent circuit, R_S represents the internal or solution resistance, including the electrolyte and intrinsic resistance of the electrode material. The R_{CT} element corresponds to the charge-transfer resistance at the electrode/electrolyte interface, reflecting the kinetics of Faradaic reactions. The C_{dl} (double-layer capacitance) describes the electrostatic charge storage at the interface between the electrode surface and the electrolyte. The Z_W (Warburg impedance) is associated with ion diffusion within the porous structure of the electrode and becomes significant at low frequencies.

For an ideal capacitor, we would expect a vertical line (phase angle = 90°); however, our samples have been shown to exhibit certain pseudocapacitive properties (i.e., some redox peaks). Due to this, in the mid-range region, we see the semicircle (after cycling, it resembles a Constant Phase Element (CPE); however, for fitting purposes, a capacitor was used), where, on top of double-layer charging, we also see the dominance of charge-transfer resistance. That being said, this part is relatively small for our samples, suggesting limited redox reactions in the electrode. The relative absence of these reactions could also be responsible for the longevity of this particular sample. The pre- and post-cycling EIS values are presented in a table below. The results paint quite an interesting picture. The incorporation of carbonaceous materials clearly enhances electrode performance, as the initial capacity increases by more than an order of magnitude. The addition of conductive components also reduces the overall resistance, while the charge-transfer resistance associated with redox processes involving Co and Mn species remains relatively low. The presence of these additives proves beneficial during cycling: the composite electrodes exhibit nearly constant resistance, whereas the pure oxide samples show a pronounced increase (in the CV-cycled sample R_{CT} almost doubles).

Table 1. Parameters calculated from EIS by fitting the data to the equivalent circuit presented in Fig. 6.

Electrode/cycling mode	Freshly prepared			After cycling		
	R_{CT}/ohm	C_{DL}/F	R_1/ohm	R_{CT}/ohm	C_{DL}/F	R_1/ohm
1 CV (PEDOT+MNO_2/Co_3O_4)	1.03	$8.42*10^{-5}$	65.80	2.01	$2.57*10^{-5}$	119.48
1 GCD (PEDOT+MNO_2/Co_3O_4)	1.39	$5.69 * 10^{-5}$	55.83	1.79	$2.41 * 10^{-5}$	202.32
2 CV (PEDOT+MNO_2/Co_3O_4/CNT)	1.45	$1.29 * 10^{-4}$	24.72	1.79	$6.62 * 10^{-5}$	33.70
2 GCD (PEDOT+MNO_2/Co_3O_4/CNT)	1.37	$1.37 * 10^{-4}$	42.69	1.49	$1.3 *10^{-4}$	71.26
3 CV (PEDOT+MNO_2/Co_3O_4/CNT/GO)	1.14	$1.83 * 10^{-4}$	43.85	1.48	$6.82 * 10^{-5}$	33.85
3 GCD (PEDOT+MNO_2/Co_3O_4/CNT/GO)	1.81	$1.08 * 10^{-4}$	51.75	1.75	$1.19 *10^{-4}$	39.67

Further insights are obtained from the evolution of R1. In the first sample, this resistance increases nearly fourfold after GCD cycling, indicating significant degradation of the active material and the accumulation of electrochemically inactive species on the surface, which hinder charge-transfer processes. The GCD and CV data support this interpretation, as these samples (1-CV and GCD) display the highest capacity fading, consistent with surface degradation or dissolution. The addition of CNTs offers marginal improvement, resulting in a modest resistance increase of ca. 30%. Further addition of GO enhances structural stability, as evidenced by a decrease in R_1, likely related to surface preservation and the removal of synthesis by-products.

The influence of cycling mode also reveals a consistent pattern. CV cycling accelerates material degradation, leading to higher resistances and reduced double-layer capacitance. Under GCD cycling, these changes are less pronounced and depend on the presence of carbon additives. The sample containing both CNT and GO remains essentially unchanged during cycling. The minor improvement falls within experimental error.

Conclusion

A hybrid electrode material composed of MnO_2, Co_3O_4, and a carbon framework was successfully synthesized and electrochemically characterized. The study demonstrated that including graphene oxide (GO) in the composite formulation yields improved electrochemical behavior. The GO-contained composite exhibited remarkable cycling stability, evidenced by the consistent CV and GCD responses over 5000 numerous cycles.

Thermal analysis using TGA revealed that the GO-containing composite exhibited slightly lower residual mass and thermal stability, likely due to the decomposition of oxygen-rich functional groups. Nevertheless, this characteristic can be considered advantageous, as it highlights the role of GO in tailoring the composite structure. These findings support the hypothesis that careful engineering of the composite (e.g., with controlled GO content) may be highly beneficial for practical supercapacitor applications, particularly within the standard operating temperature range (~60–80 °C).

Synergy between the redox-active transition metal oxides and conductive polymer embedded in a high-surface-area carbon framework enables efficient charge transport and mechanical resilience. The PEDOT + MnO_2/Co_3O_4/Carbon framework composite electrode, developed via a simple and cost-effective one-step synthesis method, stands out as a highly promising material for next-generation supercapacitors. This streamlined fabrication process not only reduces production complexity and cost, but also avoids the use of hazardous chemicals and multi-stage treatments, making it safer and more environmentally friendly. The resulting composite exhibits excellent structural integration and electrochemical performance, demonstrating that high-efficiency energy storage materials can be achieved through sustainable and scalable approaches. This work highlights a viable pathway toward practical, low-cost, and high-performance supercapacitor technologies.

Future studies will focus on exploiting the simplicity of the proposed synthesis route, which provides wide opportunities for further optimization. In particular, attention will be given to adjusting the compositional ratios of the powder constituents and incorporating additional components to enhance the electrochemical performance and stability of the electrodes.

Acknowledgements. This research [grant № PHDF - 23-1014] has been supported by Shota Rustaveli National Science Foundation of Georgia (SRNSFG).

Authors' contributions. A.Benashvili: experimental investigation, original draft preparation and writing. **N.Nioradze:** conceptualization, methodology, final review and editing. **D.Tediashvili:** improved overall paper mistakes, worked on figures and table. **L.Rokva:** corrected grammar mistakes.

Abbreviations

PEDOT: Poly(3,4-ethylenedioxythiophene)
EDS: Energy Dispersive X-ray spectroscopy
XRD: X-ray diffraction
CV: Cyclic Voltammetry
GCD: Galvanic Charge/Discharge
EIS: Electrochemical Impedance Spectroscopy
EDLC: Electric Double-layer Capacitor
TMO: Transition Metal Oxide
CNT: Carbon nanotube
PANI: Polyaniline
PPy: Polypyrrole
GO: graphene oxide
SA-ECNF: Superaligned electrospun carbon nanofiber
TGA: thermal gravimetric analysis
XRF: X-ray fluorescence
DTA: Differential Thermal Analysis
TG: Thermogravimetry
ECSA: Electrochemically Active Surface Area
CPE: Constant Phase Element

References

1. Liang R., Du Y., Xiao P., Cheng J., Yuan S., Chen Y., Yuan J., Chen J. Transition metal oxide electrode materials for supercapacitors: A review of recent developments. *Nanomaterials*, 2021, **Vol. 11,** p. 1248. DOI: 10.3390/nano11051248.
2. Jayakumar S., et al. A comprehensive review of metal oxides (RuO_2, Co_3O_4, MnO_2 and NiO) for supercapacitor applications and global market trends. *J. Alloys Compd*., 2024, **Vol. 976,** p. 173170. DOI: 10.1016/j.jallcom.2023.173170.
3. Lai C.H., Lu M.Y., Chen L.J. Metal sulfide nanostructures: Synthesis, properties and applications in energy conversion and storage. *J. Mater. Chem*., 2012, **Vol. 22,** p. 21968–21976. DOI: 10.1039/c1jm13879k.
4. Wu D., Xie X., Zhang Y., Zhang D., Du W., Zhang X., Wang B. MnO_2/carbon composites for supercapacitor: Synthesis and electrochemical performance. *Front. Mater*., 2020, **Vol. 7,** p. 2. DOI: 10.3389/fmats.2020.00002.
5. Wang X., Fu J., Wang Q., Dong Z., Wang X., Hu A., Wang W., Yang S. Preparation and electrochemical properties of Co_3O_4 supercapacitor electrode materials. *Crystals*., 2020, **Vol. 10,** p. 720. DOI: 10.3390/cryst10090720.
6. Wang X.M., Yin S.M., Jiang J., Xiao H.P., Li X.H. A tightly packed Co3O4/C&S composite for high-performance electrochemical supercapacitors from a cobalt (III) cluster-based coordination precursor. *J. Solid State Chem*., 2020, **Vol. 288,** p. 121435.
7. Lu J.L., Li J.E., Wan J., Han X.Y., Ji P.Y., Luo S., Gu M.X., Wei D.P., Hu C.G. A facile strategy of in-situ anchoring of Co_3O_4 on N doped carbon cloth for an ultrahigh electrochemical performance. *Nano Research*., 2021, **Vol. 14(7),** p. 2410-2417. DOI: 10.1007/s12274-019-3242-6.
8. Tadesse M.G., Ahmmed A.S., Lübben J.F. Review on conductive polymer composites for supercapacitor applications. *J. Compos. Sci*., 2024, **Vol. 8,** p. 53. DOI: 10.3390/jcs8020053.
9. Usman M., et al. Nickel foam–graphene/MnO_2/PANI nanocomposite based electrode material for efficient supercapacitors. *J. Mater. Res*., 2015, **Vol. 30(21),** p. 3192–3200. DOI: 10.1557/jmr.2015.271.
10. Stoller M.D., Ruoff R.S. Best practice methods for determining an electrode material's performance for ultracapacitors. *Energy & Environmental Science*, 2010, **Vol. 3(9),** p. 1294–1301. DOI: 10.1039/c0ee00074d
11. Majumdar D. Review on current progress of MnO_2-based ternary nanocomposites for supercapacitor applications. *ChemElectroChem*., 2021, **Vol. 8(2),** p. 291–336**,**. DOI: 10.1002/celc.202001371.
12. Liu J., Jiang J., Cheng C., Li H., Zhang J., Gong H., Fan H.J. Co_3O_4 nanowire@MnO_2 ultrathin nanosheet core/shell arrays: A new class of high-performance pseudocapacitive materials. *Adv. Mater*., **Vol. 23(18)**, p. 2076–2081. 2011. DOI: 10.1002/adma.201100058.
13. Roy H.S., Islam M.M., Mollah M.Y.A., Susan M.A.B.H. Polyaniline–MnO_2 composites prepared in situ during oxidative polymerization of aniline for supercapacitor applications. *Mater. Today Proc*., 2020, **Vol. 29,** p. 1013–1019. DOI: 10.1016/j.matpr.2020.04.635.
14. Tian Q., Wang X., Huang G., Guo X. Nanostructured (Co, Mn)$_3O_4$ for high capacitive supercapacitor applications. *Nanoscale Res. Lett*., 2017, **Vol. 12,** p. 214. DOI: 10.1186/s11671-017-1977-0.
15. Obodo R.M., Nsude H.E., Eze C.U., Okereke B.O., Ezugwu S.C., Ahmad I., Maaza M., Ezema F.I. Optimization of MnO_2, NiO and MnO_2@NiO electrodes using graphene oxide for supercapacitor applications. *Curr. Res. Green Sustain. Chem*., 2022, **Vol. 5,** 100345. DOI: 10.1016/j.crgsc.2022.100345.
16. Allado K., Liu M., Jayapalan A., Arvapalli D.M., Nowlin K., Wei J. Binary MnO_2/Co_3O_4 metal oxides wrapped on superaligned electrospun carbon nanofibers as binder-free supercapacitor electrodes. *Energy Fuels*, 2021, **Vol. 35,** p. 8396–8405. DOI: 10.1021/acs.energyfuels.1c00556.

17. Mahmudi W., Widiyastuti, Nurlilasari P., Affandi S., Setiawan H. Electrolysis synthesis of MnO_2 in acidic environment and its electrochemical performance for supercapacitor. *J. Phys. Conf. Ser.*, 2018, **Vol. 1093**, 012021. DOI: 10.1088/1742-6596/1093/1/012021.
18. Chen H., **Yang M., Liu Y., Yue J., Chen G.** Influence of Co_3O_4 nanostructure morphology on the catalytic degradation of p-nitrophenol. *Molecules*, 2023, **Vol. 28.** 7396. DOI: 10.3390/molecules28217396.
19. Manjula N., Chen S.M. Simple strategy synthesis of manganese cobalt oxide anchored on graphene oxide composite as an efficient electrocatalyst for hazardous 4-nitrophenol detection in toxic tannery waste. *Microchem. J.*, 2021, **Vol. 168,** 106514. DOI: 10.1016/j.microc.2021.106514.
20. Balakrishnan R., Sivasubramanian V., Gnanasekaran T., Ramasamy P., Rajendran S., Venkatesan M. Solid-state synthesis of transition metal oxides, including MnO_2/Co_3O_4 composites, by co-precipitation followed by calcination at 700 °C. *Solid State Sci*., 2024, **Vol. 12,** p. 45–58. DOI: 10.1016/j.solidstatesciences.2024.106999.
21. Li T., Li S., Zhang B., Wang B., Chen Z., Yan Y., Wan N., Zhang W. Supercapacitor electrode with a homogeneously Co_3O_4-coated multiwalled carbon nanotube for a high capacitance. *Nanoscale Res. Lett*., 2015, **Vol. 10**, p. 91. DOI: 10.1186/s11671-015-0915-2.
22. Iqra T., Riaz T., Shahzadi T., Zaib M., Qamar M.T. Fabrication of novel CMC-supported MnO_2/Co_3O_4 nanocomposite to explore its potential for treatment of MOX-contaminated water. *Polym. Plast. Technol. Mater.,* 2025, **Vol. 64,** p. 1–12. DOI: 10.1080/25740881.2025.2467266.
23. Worku A.K., Ayele D.W., Habtu N.G., Yemata T.A. Engineering Co_3O_4/MnO_2 nanocomposite materials for oxygen reduction electrocatalysis. *Heliyon*, 2021, **Vol. 7,** e08076. DOI: 10.1016/j.heliyon.2021.e08076.
24. Mohamed M.A., Galwey A.K., Halawy S.A. The activities of some metal oxides in promoting the thermal decomposition of potassium oxalate. *Thermochim. Acta*., 2002, **Vol. 387,** p. 63–74.
25. Olcay R.H., Reyes I.A., Palacios E.G., García-Hernández L., Ramírez-Ortega P.A., Ordoñez S., Juárez J.C., Reyes M., González-Islas J.C., Flores M.U. Kinetics of thermal decomposition of carbon nanotubes decorated with magnetite nanoparticles. *J. Carbon Res*., 2024, **Vol. 10,** p. 96. DOI: 10.3390/c10040096.
26. Elgrishi N., Rountree K.J., McCarthy B.D., Rountree E.S., Eisenhart T.T., Dempsey J.L. A practical beginner's guide to cyclic voltammetry. *J. Chem. Educ*., 2018, **Vol. 95,** p. 197–206. DOI: 10.1021/acs.jchemed.7b00361.
27. Lipus J., Krukiewicz K. Challenges and limitations of using charge storage capacity to assess capacitance of biomedical electrodes. *Measurement.,* 2022, **Vol. 191**, 110822. DOI: 10.1016/j.measurement.2022.110822.
28. Zhang L., Zhao X., Lv W. Why cyclic voltammetry overestimates capacitance in supercapacitors: A critical review. *Electrochim. Acta*., 2019, **Vol. 296,** p. 1005–1013. DOI: 10.1016/j.electacta.2018.11.104.
29. Wang G., Zhang L., Zhang J. A review of electrode materials for electrochemical supercapacitors. *Chem. Soc. Rev.,* 2012, **Vol. 41,** p. 797–828. DOI: 10.1039/C1CS15060J.
30. Gittins J.W., et al. Interlaboratory study assessing the analysis of supercapacitor electrochemistry data. *J. Power Sources*, 2023, **Vol. 585,** 233637. DOI: 10.1016/j.jpowsour.2023.233637.
31. Mainka J., Gao W., He N., Dillet J., Lottin O. A general equivalent electrical circuit model for the characterization of MXene/graphene oxide hybrid-fiber supercapacitors by electrochemical impedance spectroscopy – impact of fiber length. *Electrochim. Acta*, 2022**, Vol. 404,** 139740. DOI: 10.1016/j.electacta.2021.139740.
32. Sharma S., Chand P. Supercapacitor and electrochemical techniques: A brief review. *Results Chem*., 2023, **Vol. 5,** 100885. DOI: 10.1016/j.rechem.2023.100885.
33. Rus-Casas C., Ramos-Paja C.A., Serna-Garcés S.I., Gilabert-Torres C., Aguilar-Peña J.D. A circuital equivalent for supercapacitors accurate simulation in power electronics systems. *Batteries*., 2025, **Vol. 11(8),** 307. DOI: 10.3390/batteries11080307.